Available online at www.sciencedirect.com
ScienceDirect
Journal of the European Ceramic Society 27 (2007) 2697–2703
www.elsevier.com/locate/jeurceramsoc

Fe speciation in geopolymers with Si/Al molar ratio of ~2

Dan S. Perera [a,*], John D. Cashion [b], Mark G. Blackford [a], Zhaoming Zhang [a], Eric R. Vance [a]

[a] *Institute of Materials and Engineering Science, Australian Nuclear Science and Technology Organisation, PMB 1, Menai, NSW 2234, Australia*
[b] *School of Physics, Monash University, Clayton, Vic. 3800, Australia*

Received 22 June 2006; received in revised form 12 September 2006; accepted 7 October 2006
Available online 11 December 2006

Abstract

The speciation of Fe was studied in metakaolin-based geopolymers to which Fe was added as ferric nitrate solution or freshly precipitated ferric hydroxide. From Mössbauer and near-edge X-ray absorption spectroscopies, coupled with X-ray diffraction and electron microscopy, it was concluded that in as-cured geopolymers the Fe was present in octahedral sites, either as isolated ions in the geopolymer matrix or as oxyhydroxide aggregates which had not reacted with the starting geopolymer components. For material to which iron nitrate was added, heating to 900 °C allowed the formation of nepheline and a glass, both of which contained tetrahedrally coordinated, substituted Fe^{3+}.

Keywords: Electron microscopy; Spectroscopy; X-ray methods; Geopolymers; Alkali oxides

1. Introduction

Geopolymers (GPs) with Si/Al molar ratios of ~2 are alkali aluminosilicate materials[1,2] which can be made at near ambient temperatures and are X-ray amorphous. They are composed of cross-linked $[AlO_4]^-$ and $[SiO_4]$ tetrahedra, with charge balancing Na^+ or K^+ ions. They are made by exposing reactive aluminosilicate precursors such as fly ash, blast furnace slags or metakaolin (MK) to alkali solutions, with or without silicate, with minimum water addition to make a stiff paste. The mixtures polymerise and solidify upon curing at 20–90 °C, preferably in high humidity and sealed conditions. Their main potential applications are as building materials and a limited number of buildings have been constructed.[3] Geopolymers are very heat-resistant compared with Portland cement and also have the potential capability to incorporate and immobilise a variety of radioactive waste ions, including Sr and Cs,[4–7] as well as mining waste which invariably consists of various minerals containing Ti, Mn, Fe and Ca among many others.[8,9] A brief overview has been reported on the speciation of these elements in GPs.[10]

Iron can be a major component of mining wastes and it can exist in many forms, but it would be more likely to affect the kinetics and overall chemistry of geopolymer formation if the iron was in a relatively soluble form. As part of this approach, the speciation of iron in an MK-based geopolymer has been studied in some detail in the present work. The basic approach taken was to introduce ferric iron, either as a soluble salt or as freshly precipitated (oxy)hydroxide, to maximise the potential mobility of the Fe in the wet preparation.

2. Experimental

GPs having Si/Al and Na/Al molar ratios of 2.0 and 1.0, respectively were prepared with the necessary additives as listed in Table 1. The molar ratio of water to sodium was 7.2:1. The ferric (oxy)hydroxide was freshly prepared by adding NaOH solution to a solution of $Fe(NO_3)_3{\cdot}9H_2O$; the precipitate was filtered and washed with deionised water five times to remove sodium nitrate. The expected product should be either ferrihydrite, $Fe_5HO_8{\cdot}4H_2O$, or goethite, α-FeOOH, depending on the speed of reaction.[11] The dried precipitate was analysed by powder X-ray diffraction (XRD, see below) and the pattern was very diffuse, but in basic agreement with that of a two-line ferrihydrite pattern.[12]

The (oxy)hydroxide or the nitrate solution was mixed well with the MK in a pestle and mortar for about 10 min before adding to the solution of sodium silicate and water. After mixing for 5 min, the slurry was poured into a 40 mm polycarbonate

* Corresponding author. Fax: +61 2 9543 7179.
E-mail address: dsp@ansto.gov.au (D.S. Perera).

0955-2219/$ – see front matter.
doi:10.1016/j.jeurceramsoc.2006.10.006

Table 1
Composition of the baseline composition and the additives

Precursor	Mass%
Sodium silicate solution (Type D, PQ Corporation, Australia)—14.7 Na_2O, 29.4 SiO_2, 55.9 H_2O (mass%)	63.0
Metakaolin (heated Kingwhite clay, Unimin Australia Ltd., at 750 °C for 15 h)	33.7
Extra deionised water	3.3
$Fe(OH)_3$—freshly prepared (for details see the text)	1 and 5[a]
$Fe(NO_3)_3{\cdot}9H_2O$ (Sigma–Aldrich Australia Ltd.)	1[a]

[a] Added to 100% baseline composition as equivalent Fe_2O_3.

cylindrical jar and covered with a screw cap. This was shaken for 5 min on a vibrating table to de-air. Each batch weighed ~20 g and had dimensions of ~40 mm diameter × 10 mm thick. They were cured at ambient for 24 h followed by curing at 60 °C for 24 h (closed container) and removed from the jar after 3 days. All the GPs were older than 7 days when subjected to further experimentation, to maximise the chances of complete polymerisation.

The samples to which the ferric nitrate was added were heated in air to 600, 700, 800 and 900 °C for 2 h in an electric furnace. Heating and cooling rates were 5 °C/min.

All samples were analysed by XRD (Model D500, Siemens, Karlsruhe, Germany) using Co Kα radiation on crushed portions of material. Selected samples were cross sectioned, mounted in epoxy resin, and polished to a 0.25 μm diamond finish and examined by scanning electron microscopy (SEM: Model 6400, JEOL, Tokyo, Japan) operated at 15 kV and fitted with an X-ray microanalysis system (EDS: Model: Voyager IV, Tracor Northern, Middleton, WI, USA).

Transmission electron microscopy (TEM) and EDS analysis were performed using a JEM 2000fxII (JEOL, Japan) machine with a LaB_6 electron source operated at 200 kV. The TEM was equipped with a LINK energy dispersive X-ray spectrometer and ISIS microanalysis system (both from Oxford Instruments, UK). The Cliff–Lorimer method[13] was used to analyse energy dispersive spectra with experimental correction factors determined from a suite of natural mineral and synthetic ceramic materials of known composition. A Model 636 double tilt liquid nitrogen cooled specimen holder and a Model 613-0500 cold stage controller (both from Gatan, USA) were used for TEM/EDS analyses.

Care was taken to minimise electron beam damage during EDS analyses by cooling the sample to liquid nitrogen temperature and by ensuring the electron beam was never focussed below 200 nm diameter. Despite these precautions the measured sodium content was significantly lower than expected, most likely due to Na migration caused by the electron beam.

X-ray absorption near-edge structure (XANES) measurements were carried out at beamline 24A, National Synchrotron Radiation Research Centre (NSRRC), Hsinchu, Taiwan.[14] The powdered samples were spread on double-sided copper tape and mounted on a stainless steel sample holder. Fe L-edge X-ray absorption spectra were taken in the total-electron yield (TEY) mode by monitoring the specimen current.

Mössbauer spectroscopic analysis of the iron phases was carried out at room temperature using a conventional constant acceleration drive and a $^{57}CoRh$ source. Velocity calibration was carried out with α-Fe and all isomer shifts are quoted relative to α-Fe at room temperature. Fitting was carried out by conventional least squares techniques, with the intensities and linewidths of doublet lines, and also the corresponding lines of sextets, constrained to be equal. In the sextet fitting, it was also assumed that the hyperfine field and the electric field gradient were collinear.

3. Results and discussion

3.1. X-ray diffraction

Table 2 lists XRD analyses for all the GPs made, including the heating results and the sample to which iron nitrate was added. The XRD traces of all GPs indicated the presence of an amorphous phase by the broad diffuse peak centred at ~0.32 nm (see Fig. 1), together with weak peaks due to crystalline anatase and quartz impurities in the MK, as observed by other workers on MK-based geopolymers.[15] These impurities in the original clay were estimated at ~1 mass% (see Figs. 1 and 2).

When Fe is added as the (stable) nitrate to the geopolymer mixture, Fe (oxy)hydroxide would likely precipitate in

Table 2
XRD analyses of heated and unheated GPs

Equivalent Fe_2O_3 equivalent additions to GPs (mass%)	Heat treatment (°C)	XRD analysis
1 (hydroxide)	22	Am (M), Q (m), A (m)
5 (hydroxide)	22	Am (M), Q (m), A (m), iron hydroxide (m)
1 (nitrate)	22	Am (M), Q (m), A (m), $NaNO_3$ (m)
1 (nitrate)	600	Am (M), Q (m), A (m)
1 (nitrate)	700	Am (M), Q (tr), A (tr)
1 (nitrate)[a]	800	Am (M), N (m), A (tr)
1 (nitrate)[a]	900	N (M), Am (m)

Am, amorphous; Q, quartz; A, anatase; N, nepheline; M, major; m, minor; tr, trace.

[a] 1 and 5 mass% of hydroxide when heated showed N (M) and Am (m) as phases.

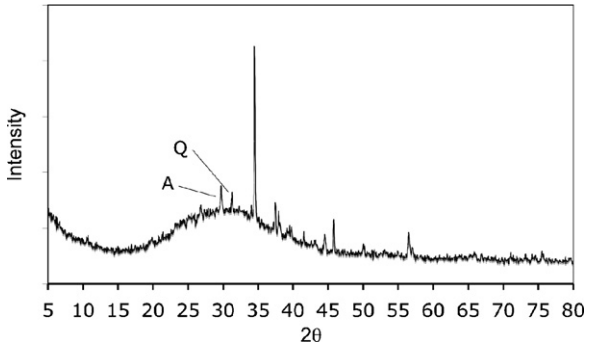

Fig. 1. XRD trace of unheated GP, containing 1 mass% equivalent Fe_2O_3 added as the nitrate (A, anatase; Q, quartz; rest, $NaNO_3$ peaks).

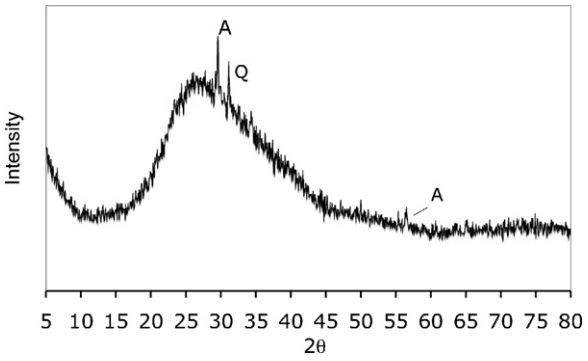

Fig. 2. XRD trace of GP, containing 1 mass% equivalent Fe_2O_3 added as the nitrate in aqueous solution and heated to 600 °C in air (A, anatase; Q, quartz).

the presence of the strong alkali solution. Soluble NO_3^- ions would remain in any aqueous phase, and XRD of the cured material showed crystalline $NaNO_3$ to be present. $NaNO_3$ was also observed when other metal nitrates were added to similar geopolymers.[6] No XRD peaks characteristic of any crystalline Fe-rich phase were observed.

After heating the sample to which iron nitrate was added, to 600–800 °C, the diffuse XRD peak gradually moved to ~0.37 nm (Fig. 2). $NaNO_3$ was not seen after this heating as it melts at ~307 °C and dissociates at ~380 °C.[16] Nepheline ($NaAlSiO_4$) was observed after heating at 800 °C and it became the major phase after heating at 900 °C as expected[17] (see Fig. 3). Liquid phase sintering takes place at ~600 °C[17] and this liquid forms a glassy phase when cooled to ambient. It is perhaps the presence of this glass that shifts the center of the diffuse peak to a slightly higher *d*-spacing than that of the unheated material. The *d*-spacings of the crystalline nepheline phase have occurred at slightly higher *d*-spacings compared to those of the pure nepheline phase which forms in equivalent Fe-free material. This is indicative of Fe^{3+} substitution in the structure, noting that Fe^{3+} has larger ionic size than Al^{3+}[18] and no X-ray evidence of other crystalline iron-bearing phases was observed.

3.2. SEM

The SEM image of the sample in which 1 mass% equivalent Fe_2O_3 was added as the hydroxide is shown in Fig. 4, where the quartz and anatase are seen in the GP matrix. Residual MK

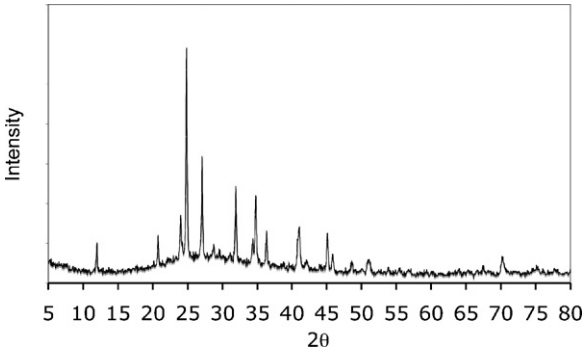

Fig. 3. XRD trace of GP, containing 1 mass% equivalent Fe_2O_3 added as the nitrate in aqueous solution and heated to 900 °C.

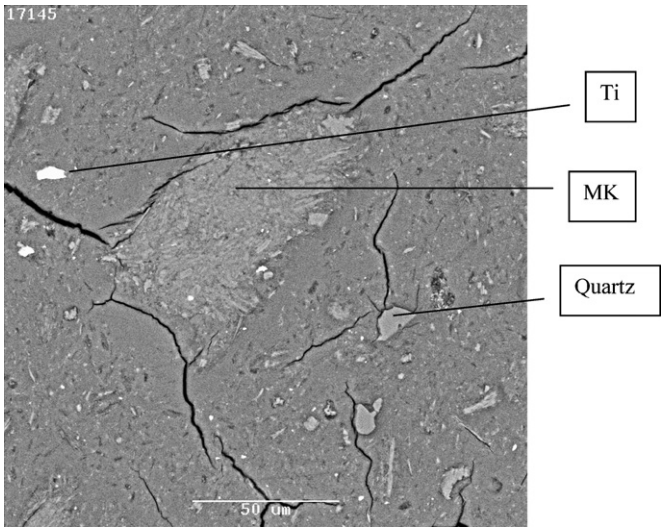

Fig. 4. Backscattered SEM image of unheated GP, containing 1 mass% equivalent Fe_2O_3 added as the hydroxide. White phase (Ti) is anatase and the lighter phase is residual MK.

is also seen which were identified by having an atomic ratio of 1 for Al:Si. The cracks observed were not present in the original GP; they resulted when the GP sample was evacuated in the SEM. Micrometre-scale inhomogeneity partly reflects the surface finish as a good polish was not obtained, due to particle pull-out. The EDS analysis of the matrix shows the presence of ~1.8 at.% Fe (Table 3). This shows that the iron is approximately uniformly incorporated into the matrix at the ~1 μm level scale of the analysis. The SEM image of the sample with 5 mass% equivalent Fe_2O_3 added as the hydroxide is shown in Fig. 5. There are some unmixed Fe-rich particles present, presumably deriving from the added Fe (oxy)hydroxide, along with the minor quartz and anatase. However, Fe-rich phases were not observed in the 1 mass% added sample (Fig. 4). The EDS analysis still showed the presence of Fe in the matrix at the ~1 μm scale but it did not reflect the increased % of Fe in the sample (Table 3). The two samples showed similar concentrations for Al and Si in the matrix, but a somewhat lower concentration for Na. However, generally it is difficult to rigorously analyse for Na in SEM because Na tends to migrate under the electron beam (see above).

For comparison, the EDS analyses (Table 3) for the sample containing 1 mass% equivalent Fe_2O_3, added as the nitrate, showed substantially less Na in the matrix than that in the Fe (oxy)hydroxide-containing GPs, perhaps because part of the Na

Table 3
SEM EDS analyses (at.%) of the GP matrices with 1 and 5 mass% equivalent Fe_2O_3 additions (unheated)[a]

Mass (%)	Na	Al	Si	Fe	Ti	O
1[b]	6.0	8.2	22.2	1.8	0.0	61.8
5[b]	7.9	8.0	21.7	0.9	0.5	61.0
1[c]	3.9	8.9	19.7	0.3	0.5	66.7

[a] Mean of ~4 spot analyses from various parts of the sample.
[b] Added as the hydroxide.
[c] Added as the nitrate.

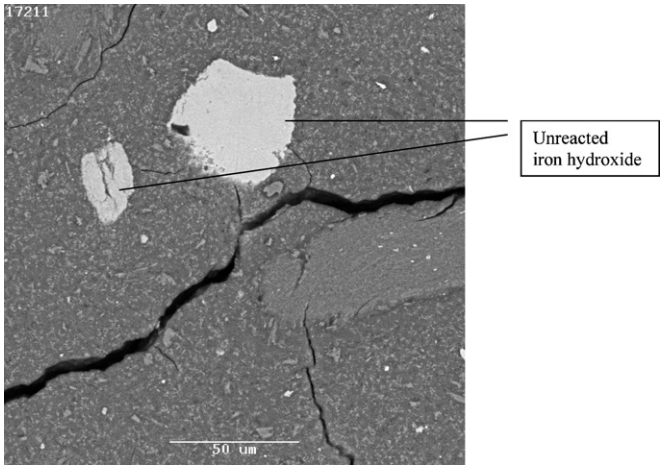

Fig. 5. Backscattered SEM image of unheated GP-containing 5 mass% equivalent Fe_2O_3 added as the hydroxide. Smaller white areas are anatase and the lighter phase is residual MK.

is present as $NaNO_3$ as shown in Table 2. $NaNO_3$, being stable, would inhabit the pore water in the GP so it is not surprising that definite areas of $NaNO_3$ were not detected in the SEM images (not shown). Although hydrous material would tend to be removed by the vacuum imposed by the SEM instrument, the Na in any residual pore water would be more likely to migrate away from the electron beam than Na incorporated in more solid material; this may explain the discrepancies between the Na contents measured by SEM in the different samples.

3.3. TEM

The TEM of the 1 mass% Fe_2O_3 equivalent (added as the nitrate) sample showed amorphous phases of the GP matrix (Fig. 6(a)), a Na-rich phase (Fig. 6(b)) and a Fe and Si-containing phase (similar to Fig. 6(a)). The EDS analyses for the GP matrix and the Fe–Si–O phase are listed in Table 4. The GP matrix phase has registered a low Na content because of Na depletion in the TEM as observed previously[19] and contains Fe. The Na-rich phase is probably the residue from the pore water after evaporation. The Fe–Si–O-containing phase (which also contains a significant amount of Al, see Table 4) is probably a reaction product or derives from the original clay used in making the MK. Its presence was not detected by XRD, although the original clay had 1 mass% Fe_2O_3 (no doubt substituting for Al) according to the supplier specification. However, the Fe–Si–O phase was found as a very minor component only in one specimen out of three examined.

Table 4
TEM EDS analyses of crystalline and amorphous phases shown in Fig. 6

Element	GP matrix		Amorphous Fe–Si–O phase	
	Element%	Atomic%	Element%	Atomic%
Na	1.2	1.1	0.9	1.4
Al	12.3	9.3	5.3	4.4
Si	32.9	24.0	23.3	19.3
Ti	0.1	0.1	0.1	0.0
Fe	3.2	1.2	27.2	11.7
O	50.3	64.3	43.2	63.2

Under the TEM, it was observed that, for the sample heated at 900 °C, crystalline material existing as the major phase was intimately associated with a glassy phase (Fig. 7(a)). Several large, well-separated grains of crystalline material were found in addition to much smaller regions of the same material (Fig. 7(b)). Fig. 8(a) is a selected area electron diffraction pattern recorded from the area shown on Fig. 7(b). Using the software package JEMS,[20] this pattern was indexed as the [0 0 1] zone axis of nepheline and an SADP (Fig. 8(b)) was simulated which closely matches the experimental pattern.

EDS spectra were recorded from the areas indicated on Fig. 7(a) and (b). The crystalline phase was electron beam sensitive and quickly became amorphous when the beam was focused onto small areas of the sample. Fig. 8 is a spectrum collected from a large area around the crystalline region shown in Fig. 7(b).

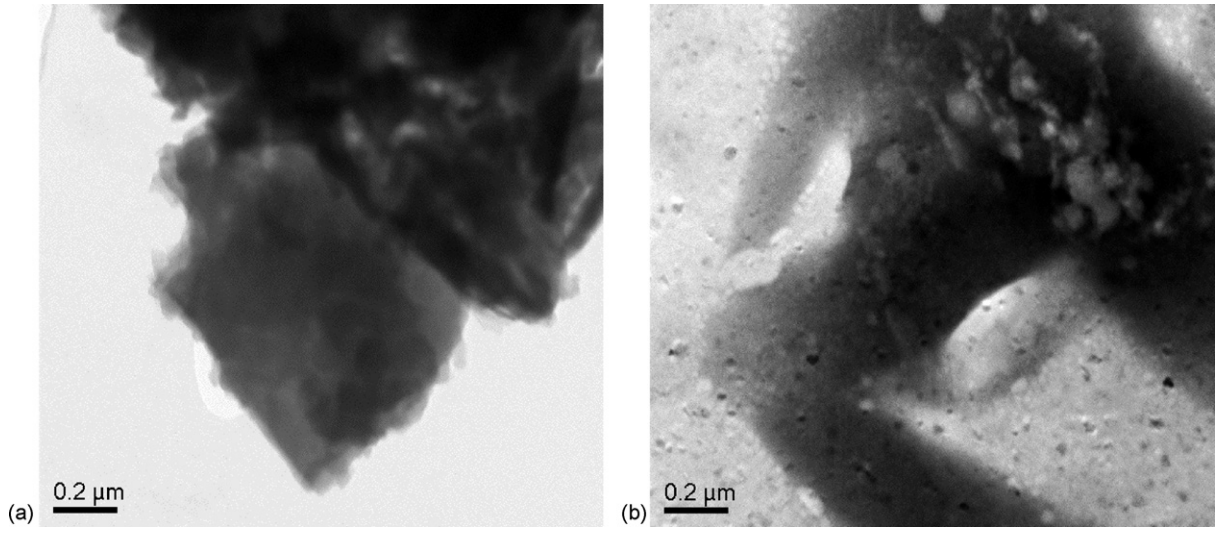

Fig. 6. TEM image of GP, containing 1 mass% equivalent Fe_2O_3 added as the nitrate in aqueous solution at ambient: (a) amorphous region of GP matrix and (b) amorphous region Na-rich area (black dots are frozen pore water).

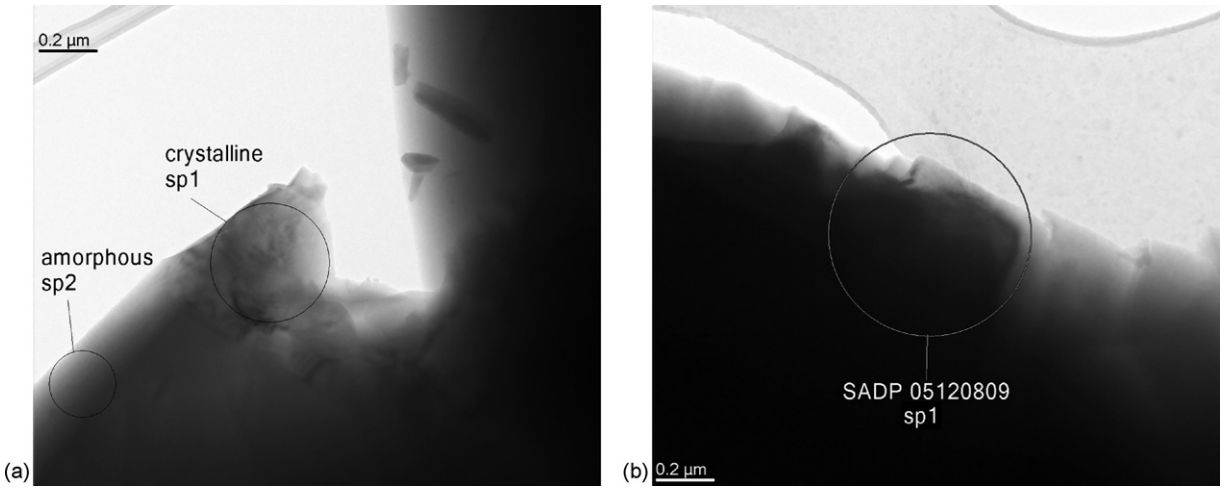

Fig. 7. TEM image of GP, containing 1 mass% equivalent Fe_2O_3 added as the nitrate in aqueous solution and heated to 900 °C: (a) crystalline and amorphous regions and (b) crystalline region only.

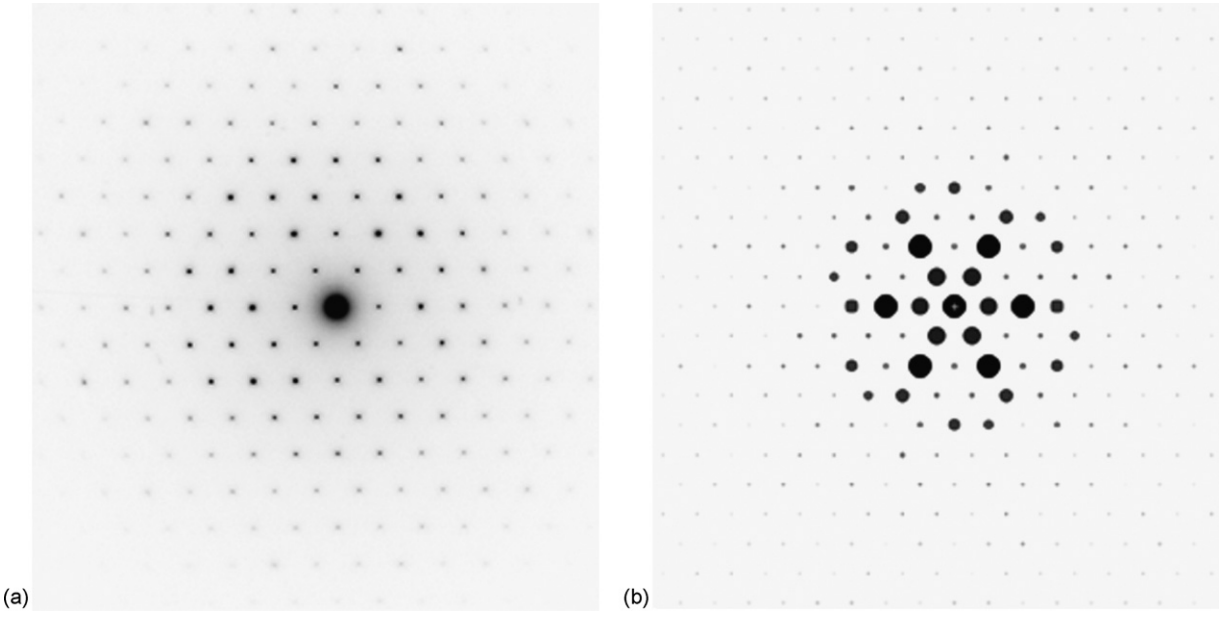

Fig. 8. (a) SADP of the crystalline area in Fig. 6(b); (b) JEMS simulated pattern.

This crystal was quite large and the beam did not need to be focused down during spectrum acquisition, hence Na depletion was minimised. The quantitative analysis of this spectrum is shown in Table 5 along with the EDS analysis for the amorphous region. The measured Fe content of the crystalline nepheline phase varies from crystal to crystal. Fe was also present in the glassy phase (Table 5).

Table 5
TEM EDS analyses of crystalline and amorphous phases shown in Fig. 7

Element	Nepheline		Amorphous phase	
	Mass%	Atomic%	Mass%	Atomic%
Na	13.6	12.2	0.3	0.2
Al	16.0	12.1	11.4	8.6
Si	22.3	16.3	35.4	25.5
K	0.2	0.1	0.2	0.1
Ti	0.3	0.1	0.3	0.1
Fe	2.2	0.8	1.3	0.5
O	45.5	58.4	51.3	65.0

The measured atomic% Na in the nepheline was very similar to that of Al (+Fe) as expected, but both were ∼20% less than that of Si. It is possible that there were unobserved admixtures of the glassy phase, which was far richer in Si than Na and Al. We note that alkali deficiencies (∼10% of the stoichiometric content) have been observed by chemical analysis (as distinct from EDS) of natural nephelines.[21]

3.4. XANES

Fig. 9 shows the Fe L-edge XANES spectrum of the Fe-doped (1 wt.% Fe added as ferric nitrate) geopolymer along with that of α-FeOOH. Both spectra have been normalised to the incoming

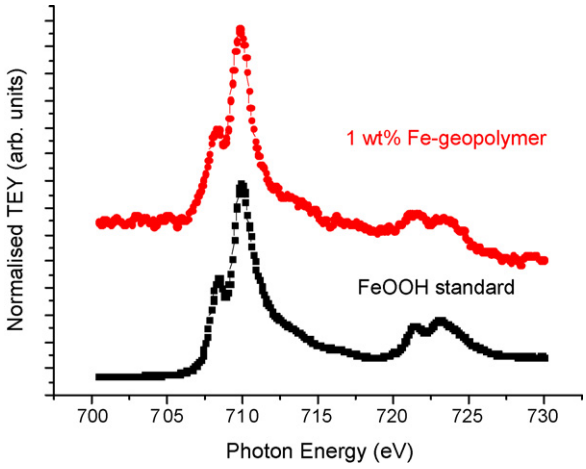

Fig. 9. Total electron yield (TEY) of Fe L-edge XANES of 1 mass% equivalent Fe_2O_3 in MKGP (red curve) and that of α-FeOOH (goethite; Fe^{3+} in octahedral coordination) for comparison. (For interpretation of the references to colour in this figure legend, the reader is referred to the web version of the article.)

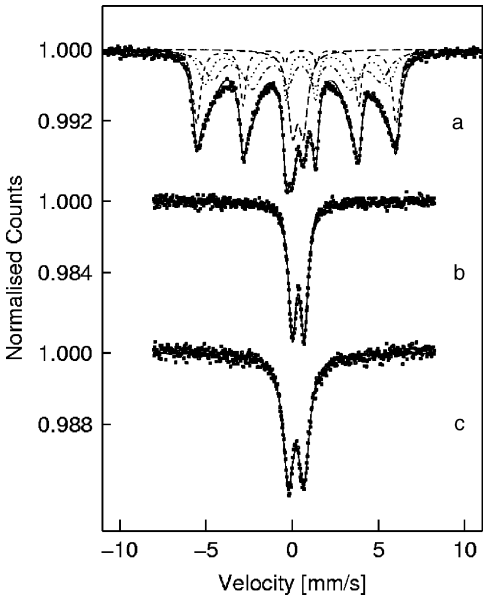

Fig. 10. Room temperature Mössbauer spectra of (a) GP sample loaded with ferric (oxy)hydroxide, (b) unheated GP sample loaded with ferric nitrate, and (c) the latter sample after heating to 800 °C.

monochromatic light intensity, which was measured using a gold mesh detector. The photon energy scale has not been calibrated against an absolute standard. The preliminary results indicate that the Fe coordination in the geopolymer sample is indistinguishable from that of octahedral Fe^{3+} in α-FeOOH (goethite), suggesting that Fe^{3+} ions were not incorporated in the Al–Si–O network, as it would then have been in tetrahedral coordination. Of course, the result only shows that the Fe is in octahedral coordination and not that the Fe is present as goethite.

3.5. Mössbauer spectroscopy

The room temperature Mössbauer spectrum of the hydroxide-loaded specimen showed a broadened magnetically split structure together with a quadrupole split doublet (Fig. 10a and Table 6). The magnetic component has been fitted to three sextets as an approximate fit to the broadened lines. The maximum hyperfine field of 35.9 T is only slightly less than the accepted room temperature value for pure goethite of 38.0 T[22] and this is the only known ferric oxyhydroxide phase with a room temperature splitting of approximately this size. The isomer shift and quadrupole splitting both agree with the literature values for goethite.[22] The doublet parameters are also consistent with those of goethite for which either the aluminium concentration or poor crystallinity has reduced the ordering temperature below ambient. The very broad linewidth is consistent with either interpretation, but the fact that no XRD evidence of crystalline goethite was observed (see above) points to poor crystallinity as being the cause.

The room temperature Mössbauer spectrum of the unheated nitrate-loaded specimen showed a quadrupole split doublet (Fig. 10b), whose isomer shift (Table 6) is consistent with iron in octahedral coordination to oxygen atoms, but the quadrupole splitting could apply to a variety of poorly crystalline ferric oxyhydroxides and is non-specific as to the exact phase. The linewidth is quite broad, indicating poor crystallinity or a variety of coordinations. The parameters are very close to those of six-line ferrihydrite (see, for example, Ref. 22, Chapter 5) and this is a likely assignment since ferrihydrite would be the expected resulting phase from the hydrolysis of ferric nitrate (see above). The data are also slightly asymmetric in the same way as for ferrihydrite, although we have fitted it with a symmetric doublet.

After the sample was heated to 800 °C, the isomer shift decreased and the quadrupole splitting increased markedly, also

Table 6
Mössbauer parameters of the spectra in Fig. 10 (for the magnetically split spectra, the quadrupole splitting is $e^2qQ/4$)

Equivalent Fe_2O_3 additions to GPs (mass%)	Heat treatment (°C)	Isomer shift (mm/s)	Quadrupole splitting (mm/s)	Hyperfine field (T)	Linewidth (mm/s)	Area (%)
5 (hydroxide)	22	0.33 (1)	0.63 (1)	0	0.62 (1)	16 (1)
		0.37 (1)	−0.12 (1)	35.9 (1)	0.44 (6)	22 (3)
		0.37 (1)	−0.13 (1)	33.0 (5)		28 (9)
		0.39 (2)	−0.13 (2)	30.2 (7)		34 (9)
1 (nitrate)	22	0.35 (1)	0.69 (1)	0	0.53 (1)	100
1 (nitrate)	800	0.23 (1)	0.90 (1)	0	0.75 (1)	100

Note: Estimated errors in parenthesis.

accompanied by an increase in the linewidth (Fig. 10c, Table 6). The isomer shift-quadrupole splitting combinations are characteristic of ferric ion in tetrahedral coordination with oxygen atoms, and almost certainly in a sodium-containing phase, as expected for Fe^{3+} substituted for Al in nepheline, all Al in nepheline being in tetrahedral coordination.[23] The systematics of the isomer shift-quadrupole splitting combinations for iron in various aluminosilicate glasses are given in Ref. 22, Section 12.2.2. Natural nepheline is not rich in iron[23] and there are no literature Mössbauer parameters for iron in nepheline. Consequently it is not possible to tell from these parameters whether the iron is in the crystalline or amorphous phases, or in both, because Fe substituting in an aluminosilicate glass would also be in tetrahedral coordination. The very broad linewidth of 0.75 mm/s strongly implies that the iron inhabits an amorphous phase, the presence of which was already deduced from the XRD and TEM results. The spectrum is also asymmetric in the way indicative of a small correlated distribution of isomer shifts and quadrupole splittings, as is common for aluminosilicate glasses,[22] although we have not been fitted it to this model. The sense of the asymmetry is opposite to that in Fig. 10b.

4. Conclusions

The speciation of Fe added as ferric nitrate solution or freshly precipitated ferric (oxy)hydroxide to metakaolinite-based geopolymers was studied and from Mössbauer and near-edge X-ray absorption spectroscopies, together with X-ray diffraction and electron microscopy, it was concluded that in as-cured geopolymers the Fe was present in octahedral sites, either as isolated ions in dilute samples or as oxyhydroxide aggregates in samples richer in Fe. Heating to 900 °C allowed the formation of nepheline, with partial substitution of Fe^{3+} for the tetrahedral Al, as well as glass which also incorporated Fe^{3+} in tetrahedral coordination.

Acknowledgements

The authors thank G. Triani and L.-J. Liang for their assistance with the XANES measurements in Taiwan. Travel to Taiwan was supported by the Australian Synchrotron Research Program, which is funded by the Commonwealth of Australia under the Major National Research Facilities Program. Our thanks are due to Joel Davis and Rachael Trautman for SEM work. This project was carried out under the auspices and with the partial financial support of the Centre for Sustainable Resource Processing, which is established and supported under the Australian Government's Cooperative Research Centres Program.

References

1. Davidovits, J., Geopolymer: inorganic polymeric new materials. *J. Therm. Anal.*, 1999, **37**, 1633–1656.
2. Davidovits, J., Chemistry of geopolymeric systems, terminology. In *Geopolymére '99, Geopolymer International Conference, Proceedings, 30 June–2 July 1999*, ed. J. Davidovits, R. Davidovits and C. James, 1999, pp. 9–39.
3. Krivenko, P., Development of alkaline cements supported by theory and practice. In *Proceedings of the GGC 2005 (International Workshop on Geopolymers and Geopolymer Concrete), September 28–29, 2005*, 2005, CD ROM, 2005, tGGC2005. pdf.
4. Khalil, M. Y. and Merz, E., Immobilization of intermediate-level wastes in geopolymers. *J. Nucl. Mater.*, 1994, **211**, 141–148.
5. Zosin, A. P., Priimak, T. I. and Avsaragov, Kh. B., Geopolymer materials based on magnesia-iron slags for normalization and storage of radioactive wastes. *Atom. Energy*, 1998, **85**, 510–514.
6. Perera, D. S., Vance, E. R., Aly, Z., Davis, J. and Nicholson, C. L., Immobilization of Cs and Sr in geopolymers with Si/Al ∼2. Environmental issues and waste management technologies in the nuclear industries XI. *Ceram. Trans.*, 2006, **176**, 91–96.
7. Fernandez-Jimenez, A., Macphee, D. E., Lachowski, E. E. and Palmo, A., Immobilization of cesium in alkaline activated fly ash matrix. *J. Nucl. Mater.*, 2005, **346**, 185–193.
8. CANMET, *Preliminary Examination of The Potential Use of Geopolymers for Use in Mine Tailings Management*. Final report, DSS contract no. 23440-6-9195/01SQ, 1998.
9. van Jaarsveld, J. G. S., Lukey, G. C., van Deventer, J. S. and Graham, A., The stabilisation of mine tailings by reactive geopolymerisation. In *Proceedings of the International Congress on Mineral Processing and Extractive Metallurgy, 11–13 September 2000*. Australasian Institute of Mining and Metallurgy, 2000, pp. 363–371.
10. Vance, E. R., Perera, D. S., Aly, Z., Blackford, M., Zhang, Y., Rowles, M. *et al.*, Solid state chemistry phenomena in geopolymers with Si/Al ∼2. In *Proceedings of the GGC 2005 (International Workshop on Geopolymers and Geopolymer Concrete), September 28–29, 2005*, 2005, CD ROM nGGC2005.pdf.
11. Cornell, R. M. and Schwertmann, U., *The Iron Oxides: Structure, Properties, Reactions, Occurrence and Uses*. VCH, Weinheim, 1996, p. 313.
12. Eggleton, R. A. and Fitzpatrick, R. W., New data and a revised structural model for ferrihydrite. *Clays Clay Miner.*, 1988, **36**, 111–124.
13. Cliff, G. and Lorimer, G. W., The quatitative analysis of thin specimens. *J. Microsc.*, 1975, **103**, 203–207.
14. Lai, L. J., Tseng, P. C., Yang, Y. W., Chung, S. C., Song, Y. F., Cheng, N. F. *et al.*, Current status of the wide-range (10–1500 eV) spherical grating monochromator beamline at SRRC. *Nucl. Instrum. Meth. Phys. Res. A*, 2001, **467–468**, 586–588.
15. Rowles, M. and O'Connor, B., Chemical optimisation of the compressive strength of aluminosilicate geopolymers synthesised by sodium silicate activation of metakaolinite. *J. Mater. Chem.*, 2003, **13**, 1161–1165.
16. Weast, R. C., ed., *Handbook of Chemistry and Physics*. 53rd ed. The Chemical Rubber Co., Cleveland, Ohio, USA, 1972, p. 139.
17. Perera, D. S., Vance, E. R., Cassidy, D. J., Blackford, M. G., Hanna, J. V., Trautman, R. L. *et al.*, The effect of heat on geopolymers made using fly ash and metakaolinite. Advances in ceramic matrix composites X. *Ceram. Trans.*, 2004, **165**, 87–94.
18. Addison, W. E., *Structural Principles in Inorganic Compounds*. Longmans, Green and Co. Ltd., London, 1967, p. 172.
19. Blackford, M. G., Hanna, J. V., Pike, K. J., Vance, E. R. and Perera, D. S., Transmission electron microscopy and nuclear magnetic resonance in geopolymers for radioactive waste immobilisation. *J. Am. Ceram. Soc.*, submitted for publication.
20. Stadelman, P., EMS—software package for electron diffraction analysis and HREM image simulation in materials science. *Ultramicroscopy*, 1987, **21**, 131–145.
21. Douray, G., Schairer, J. F. and Douray, J. D. H., Nepheline solid solution. *Mineralog. Mag.*, 1959, **32**, 93–109.
22. Murad, E., Cashion, J. and Mössbauer, *Spectroscopy of Environmental Materials and Their Industrial Utilization*. Kluwer, Dordrecht, 2004, p. 417.
23. Deer, W. A., Howie, R. A. and Zussman, J., *An Introduction to The Rock Forming Minerals*. Longman, Essex, 1966, pp. 355–366.